

Remote Optical Switch for Localized and Selective Control of Gene Interference

Somin Eunice Lee,[†] Gang Logan Liu,[‡] Franklin Kim,[†] and Luke P. Lee*[†]

Biomolecular Nanotechnology Center, Berkeley Sensor and Actuator Center, Department of Bioengineering, University of California-Berkeley, UCSF/UCB Joint Graduate Group in Bioengineering, and 3104 Micro and Nanotechnology Laboratory, Department of Electrical and Computer Engineering, University of Illinois at Urbana-Champaign, Urbana, IL 61801

Received September 4, 2008; Revised Manuscript Received December 1, 2008

ABSTRACT

Near infrared-absorbing gold nanoplasmonic particles (GNPs) are used as optical switches of gene interference and are remotely controlled using light. We have tuned optical switches to a wavelength where cellular photodamage is minimized. Optical switches are functionalized with double-stranded oligonucleotides. At desired times and at specific intracellular locations, remote optical excitation is used to liberate gene-interfering oligonucleotides. We demonstrate a novel gene-interfering technique offering spatial and temporal control, which is otherwise impossible using conventional gene-interfering techniques.

Precise control of gene interference in living cells is in critical demand^{1,2} for studying cellular signaling pathways,³ quantitative cell biology,⁴ systems biology,⁵ and molecular cell biology.⁶ In order to advance these dynamic cellular studies, nanoscale intracellular transmitter and receiver systems are required for the remote manipulation of biological systems. Remote electronic control of DNA hybridization by inductive coupling of radio frequency,⁷ photouncaging of DNA by UV light,⁸⁻¹⁰ and chromophore-based optical activation^{11,12} of biomolecules have previously been demonstrated. Enzymes¹³ and thermo-responsive polymers¹⁴ have also been used to release biomolecules from carriers. Additionally, thermal ablation has previously been used to release large plasmids from carriers using high energy^{15,16} or to destroy cells of interest.¹⁷⁻¹⁹ However, gene interference with precise spatial and temporal resolution, minimal photodamage, as well as the selective coupling of the optical transmission frequency to different nanoscale transmitters has not yet been accomplished.

Here, we present a new remote control switch of gene interference in living cells by using oligonucleotides on a nanoplasmonic carrier-based optical switch (ONCOS), short interfering oligonucleotides, and a near-infrared (NIR) laser transmitter. Gene interference by ONCOS occurs at the

translational step. In the absence of gene interference, mRNA is transcribed from DNA in the nucleus and exported out to the cytoplasm (Figure 1b). The mRNA is then translated into the corresponding amino acids. This primary sequence of amino acids then folds into its final protein structure and is transported to the proper location in the cell.

In the presence of ONCOS gene interference, optical switches are internalized within living cells (Figure S1). The material, geometry, and size of these optical switches are specifically designed for use in ONCOS. GNPs are selected because of their stable and nontoxic properties in biological applications.^{20,21} Rod-shaped GNPs have an aspect ratio (length/diameter) of 3.5, as shown in a scanning electron microscopy image in Figure 2b. Such geometry allows highly efficient photothermal conversion due to the matched resonant frequency, making it possible to activate gene release with minimized optical exposure time and low optical power. By carefully selecting the aspect ratio of these optical switches, the plasmon resonant wavelength is tuned and a corresponding light source is chosen to activate the optical switches (Figure 2a,e). Here, the aspect ratio of GNPs is selected such that the maximum light absorbance is at a wavelength in the NIR range of interest (785 nm). Since cells are essentially transparent in this wavelength regime of 800–1300 nm,¹⁷ cell damage can be minimized when the cell is exposed to the light source. By selecting the size and thus tuning the optical transmission frequency of the GNP, it is also possible to remotely activate a variety of different

* To whom correspondence should be addressed. E-mail: lplee@berkeley.edu. Phone: (510) 642-5855.

[†] University of California-Berkeley.

[‡] University of Illinois at Urbana-Champaign.

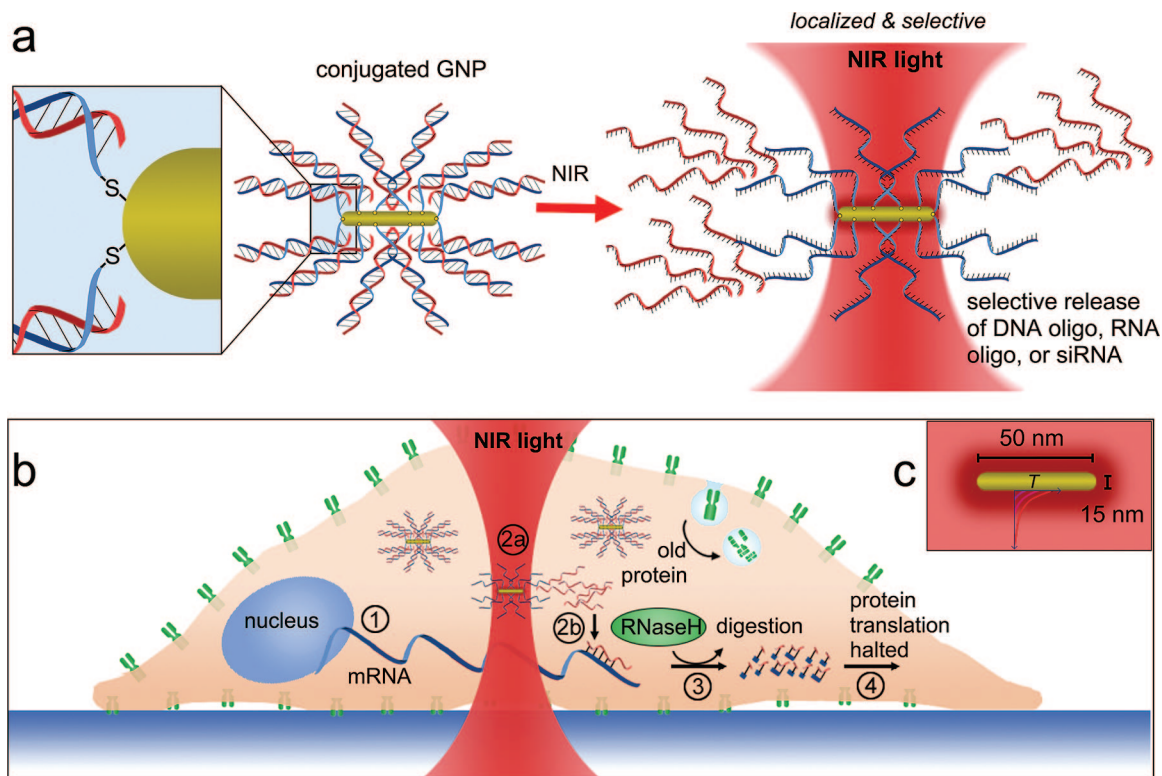


Figure 1. Concept of gene release by ONCOS activation. (a) Thiol-modified sense oligonucleotides (shown in blue) are attached to gold nanoparticle (GNP) carriers. Antisense oligonucleotides (shown in red) are then hybridized to the sense oligonucleotides. NIR illumination photothermally heats the gold carriers, causing the double-stranded oligonucleotides to denature at their melting temperature and the antisense oligonucleotides to be released from the carriers. (b) ONCOS-activated gene interference: conjugated GNPs are internalized within cells. Step 1 illustrates transcription of DNA into mRNA. Step 2a illustrates NIR activation to photothermally heat GNP carriers and release antisense oligonucleotides within the cells. Step 2b illustrates the binding of the antisense oligonucleotides to mRNA. Step 3 illustrates the digestion of the heteroduplex mRNA by RNase H enzyme, thus silencing the gene of interest at the translational step. Protein translation is halted in Step 4. Since old protein is continually degraded and no new protein is being synthesized, a decrease in the overall protein expression occurs. (c) Concept of spatially confining temperature gradient to the surface of the nanorod due to photothermal heating.

optical switches in living cells using different corresponding light sources. Finally, due to the GNPs' large surface area, each GNP is able to carry hundreds of oligonucleotides, making it possible to interfere with gene expression from the activation of a single GNP. Using the surface density of single-stranded DNA²² of 9.0×10^{12} ssDNA molecules/cm² and the dimensions of a GNP (radius = 7.5 nm, height = 50 nm), we estimate that each GNP will release approximately 250 molecules of oligonucleotides upon activation.

When the remote light source is activated, this light is absorbed by the optical switches and the resulting excess energy is dissipated in the conversion of optical energy to heat, otherwise known as the photothermal effect.^{23–28} The heat transfer from the surface of GNP to the surrounding cellular environment is highly localized and decays exponentially within a few nanometers (Figure 2c). When the minimum temperature on the optical switches reaches the melting temperature of the short duplex, the short double-stranded oligonucleotides denature. The antisense oligonucleotides are released and are allowed to bind to a portion of the corresponding mRNA (Figure 1b, part 2) while the sense oligonucleotides remain attached to the GNPs through thiol bonds. Once this mRNA/oligodeoxynucleotide heteroduplex is formed, it is recognized and degraded by RNase

H enzymes within the cell, thereby inhibiting gene translation.

As an example of localized gene interference by ONCOS, we demonstrate our method in BT474 breast carcinoma cells by optically activating the localized release of antisense oligonucleotides at a specific time and blocking the translation of the ERBB2 (also known as HER-2, neu, and EGFR-2) mRNA. Our method accomplishes gene interference with nanometer-scale spatial resolution (less than 100 nm resolution) and with temporal control. In addition, since the heat transfer from the surface of GNP exponentially decays within a few nanometers, as also previously shown using photothermal nanocrescents,^{29,30} nanoshells,¹⁷ and nanospheres,^{28,31} and nanorod-functionalized polyelectrolyte capsules,³² there is also minimal temperature disturbance to the surrounding cellular environment during gene interference of ERBB2 by ONCOS. We show that it is possible to gain highly precise spatial control and temporal tunability of translational events, which are otherwise impossible using conventional RNA interference techniques.

The first stage in demonstrating the efficacy of ONCOS involved confirming the wavelength specificity for the remote control of photothermal gene release. GNPs are prepared as previously described^{33,34} and are conjugated with double-stranded oligonucleotides and immobilized onto a glass

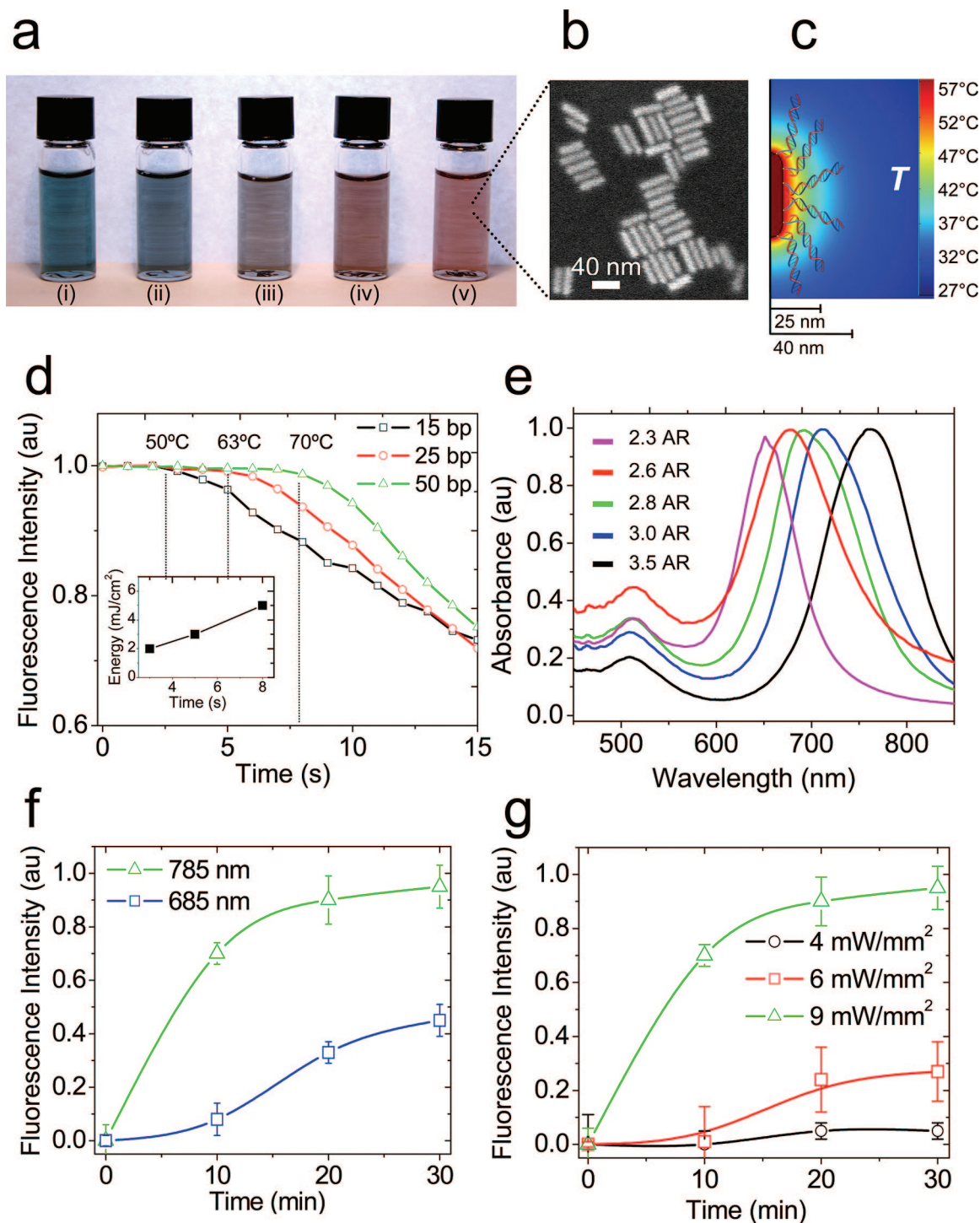


Figure 2. Experimental characterization of ONCOS activation. (a) Tunable rod-shaped GNP carriers based on different aspect ratios. Each GNP solution corresponds to a maximum absorbance (left to right): (i) 652, (ii) 676, (iii) 694, (iv) 715, and (v) 785 nm. (b) Scanning electron microscopy image showing the GNPs' aspect ratio (length/diameter) is 3.5. The aspect ratio is tuned so maximum light absorbance is at a wavelength in the NIR range of interest (785 nm). (c) Axisymmetric Femlab simulation demonstrating localized heat distribution at the GNP's surface at steady-state. (d) For experimental characterization of temperature on the nanoparticle, melting profiles for three different lengths of oligonucleotides (15, 25, and 50 bp) with known melting temperatures (50, 63, and 70 °C, respectively) are collected. Antisense oligonucleotides are FAM-labeled. Temperature is correlated to input energy by analyzing their melting profiles. (e) Absorption spectrum of tunable rod-shaped GNP carriers based on different aspect ratios (AR): (i) 2.3 AR, 652 nm, (ii) 2.6 A, 676 nm, (iii) 2.8 AR, 694 nm, (iv) 3.0 AR, 715 nm, (v) 3.5 AR, 785 nm. (f) Normalized fluorescence versus time plots comparing photothermal release for a laser at the peak optical absorption (785 nm) and a laser outside the peak optical absorption (658 nm). (g) Normalized fluorescence versus time plots comparing photothermal release for various power densities.

surface (see Materials and Methods in the Supporting Information). All the experiments are based on permanently attached nanoparticles. The antisense oligonucleotides are

labeled with fluorescent dye to visually monitor their release using fluorescence microscopy. To demonstrate wavelength specificity, a laser at the peak optical absorption (785 nm)

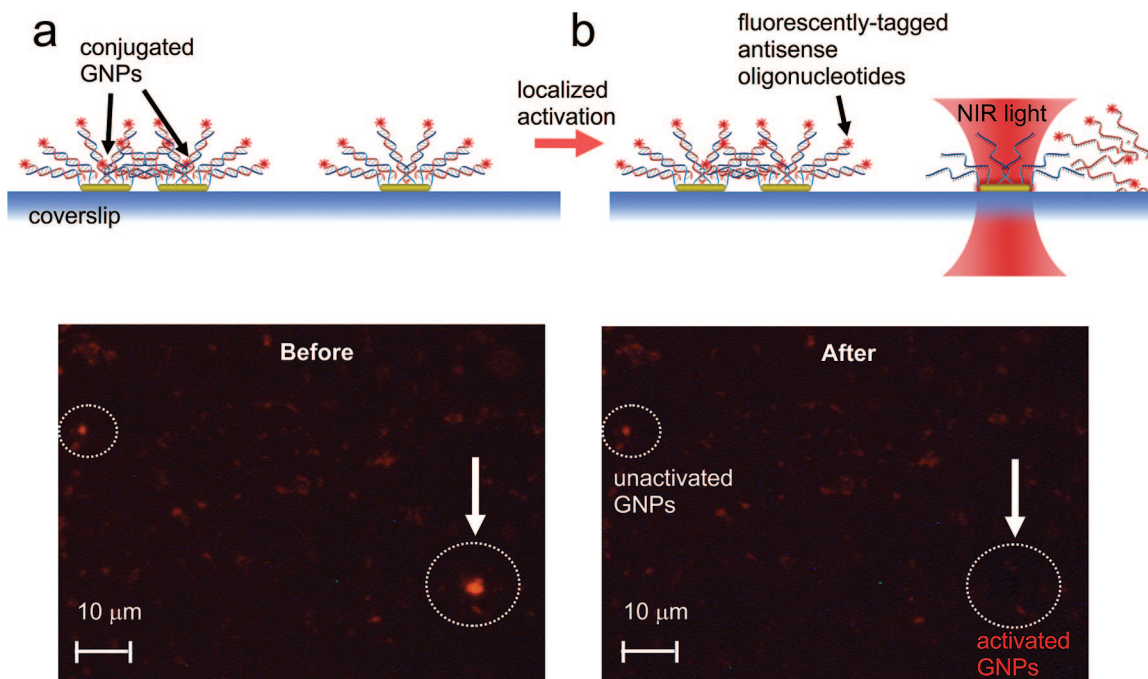


Figure 3. In vitro demonstration of gene release by ONCOS activation. Concept of localized activation of oligonucleotide release from immobilized nanoparticles. Fluorescence is from the TAMRA-labeled antisense strand of the double-stranded oligonucleotides attached to immobilized nanoparticles on glass. (a) Concept and fluorescent images before ONCOS activation. (b) Concept and fluorescence images after localized oligonucleotide release.

is compared to a laser outside the peak optical absorption (658 nm) for photothermal release. The entire viewing window is illuminated using each laser, which is positioned above the sample, and an inverted microscope operating in epi-fluorescence mode is used to visualize ONCOS gene release. Photothermal release is monitored by observing the fluorescence intensity of an area away from the conjugated GNPs. Initially, the normalized fluorescence intensity of this area is set to 0. When the temperature on the nanoparticle reaches the melting temperature of the double-stranded oligonucleotides, the antisense oligonucleotides are released and the fluorescence intensity in the observed area increases. Figure 2f shows that the photothermal efficiency is two and a half-times greater at the peak optical absorption wavelength.

To minimize laser exposure to cells, we characterized the minimal power necessary to achieve photothermal release. Conjugated GNPs, with fluorescently labeled antisense strands, are immobilized onto a glass surface and a 785 nm laser is used to illuminate the GNPs at various power densities: 4, 6, and 9 mW/mm² (see Methods in Supporting Information). Figure 2g illustrates that the photothermal efficiency rises with increasing power densities.

If ONCOS is to be used in living cells, it is important to confirm that the photothermal heat generated by ONCOS will not adversely affect them. Therefore, we characterized the temperature on the surface of the GNPs. We reasoned that if three different oligonucleotides of known length (15, 25, and 50 bp) with known melting temperatures (50, 63, and 70 °C, respectively) are photothermally melted, we could correlate the temperature on the GNPs as a function of input energy by visualizing their melting profiles. When the temperature on the GNPs reaches the melting temperature

of the oligonucleotides for each length, the fluorescent intensity decreases sharply, indicating that the antisense oligonucleotides have been released into solution. Using each profile, the energy required to reach each melting temperature is approximated by $E = \alpha Pt$, where E is the energy in J/cm², α is the absorptivity of gold, P is the power of the laser in W/cm², and t is the time in seconds (shown in inset of Figure 2d). Experimental characterization shows that melting temperatures as low as 50 °C requires 2 mJ/cm² of energy and temperatures as high as 70 °C requires 5 mJ/cm² of energy. This demonstrates that low temperature activation can be achieved with ONCOS.

In addition to experimental analysis, FEMLab software is used to simulate an axisymmetric model of the heat distribution of a single GNP at steady-state (Figure 2c). Figure 2c shows the temperature distribution as a function of distance from the surface of the GNP. From the surface of the GNP outward, the temperature profile begins at the melting temperature of the oligonucleotides and falls off exponentially to 37 °C within 100 nm from the surface of the GNP. This demonstrates that the heat generated using ONCOS is highly localized to the surface of the GNP and should not propagate significantly intracellularly. Thus, we expect that cell viability will remain uncompromised after ONCOS activation.

As a qualitative test of ONCOS' high spatial resolution, optically controlled gene release was performed both outside and inside of biological cells. Here, a NIR laser is focused to a 5 μm diameter spot size using an objective lens located above the sample. Using this focused NIR laser, certain immobilized GNPs (with fluorescently labeled antisense oligonucleotides) are illuminated while other neighboring

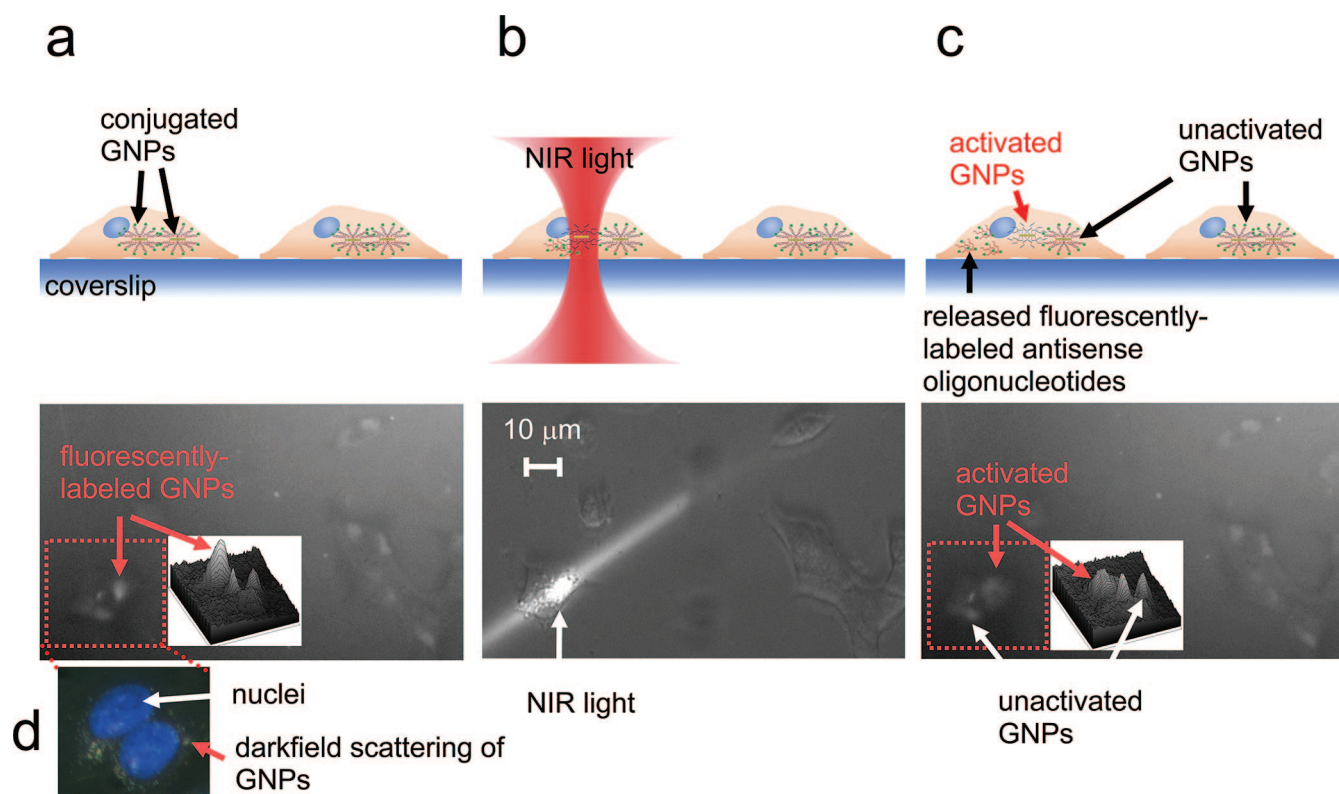


Figure 4. Visualization of intracellular ONCOS activation. Concept of localized activation of oligonucleotide release inside BT474 breast carcinoma cells. Antisense oligonucleotides are FAM-labeled. (a) Concept and fluorescence images before ONCOS activation. Inset shows surface plot of fluorescence intensity of a cell (located on the left-hand side) before ONCOS activation. (b) Concept and brightfield image of localized NIR activation. (c) Concept and fluorescent images after localized release of oligonucleotides inside BT474 breast carcinoma cells. Inset shows surface plot of fluorescence intensity of a cell (located on the left-hand side) after ONCOS activation. (d) Darkfield scattering image of single GNPs is overlaid with a DAPI-stained nuclei image to demonstrate that single GNPs congregate in groups at the nuclear membrane.

GNPs are not (Figure 3). When the temperature on the GNPs reaches the melting temperature, the antisense oligonucleotides are released into solution and the fluorescence intensity on the illuminated GNPs vanish (Figure 3b).

Having established that oligonucleotides can be released in a highly localized manner, we investigated the localized release of oligonucleotides within BT474 breast carcinoma cells by using fluorescently labeled oligonucleotides. GNPs functionalized with fluorescently labeled antisense strands, form complexes with a commercially available lipid which will undergo repulsive membrane acidolysis in a weakly acidic environment.^{35–37} The complexes are then internalized within a population of cells via endocytosis. Once inside endosomes, the lipid complexes are destabilized due to repulsive electrostatic forces generated in the weakly acidic endosomal environment, and finally, due to osmotic disruption, the endosomal membrane is broken. At this point, the functionalized GNPs are released into the cytosol and ready for use in ONCOS. Alternatively, it is also possible that by photothermally heating GNPs inside endosomes, the endosomal membrane can be disrupted and the contents can be released from the endosomes.³⁸ In Figure 4d, a darkfield scattering image of single GNPs is overlaid with a DAPI-stained nuclei image to demonstrate that single GNPs congregate in groups at the nuclear membrane. Using a highly sensitive monochromatic camera, Figure 4a shows

fluorescing functionalized GNPs internalized within cells. Because of the diffraction limit, single, closely congregated fluorescent GNPs cannot be distinguished and the GNP groups therefore appear as fluorescent “patches” or spots around the nuclei. A surface plot of the fluorescent intensity is shown as an inset in Figure 4a to clearly visualize each of the fluorescent “patches.” Control experiments were carried out to verify that cells lacking the fluorescently labeled antisense strands do not show similar fluorescence.

To show localized photothermal gene release, a focused NIR laser is used to illuminate a specific fluorescent patch within the cells, as shown in the brightfield image in Figure 4b. To ensure that oligonucleotides are well-dispersed in the cells after ONCOS activation, the illumination time was chosen such that it was longer than the estimated diffusion time of the oligonucleotides. During illumination, no oligonucleotide back-binding of released oligonucleotides onto the GNPs occurs due to the elevated temperature at the surface of the GNPs. We expect the diffusion time to be approximately 30 s, assuming that the diffusion length is approximated by the diameter of the cell (10^{-5} m) and the diffusion coefficient is 3×10^{12} m²/s for a 100 bp oligonucleotide.³⁹ Therefore, the cells were illuminated for 2 min at 9 mW/mm² to allow enough time for oligonucleotides to be well dispersed in the cytoplasm.

Upon illumination, when the temperature reaches the melting temperature, the double-stranded oligonucleotides denature and the labeled antisense strands diffuse around the cytosol as shown in Figure 4c. A surface plot of the fluorescence intensity is shown as an inset in Figure 4c to clearly demonstrate the decrease in intensity at the illuminated location while other surrounding fluorescent patches remain unaffected. The surface plot in Figure 4c compared with the surface plot in Figure 4a shows that at the activated patch, the maximum peak fluorescence intensity decreases and broadens out as the released fluorescently labeled oligonucleotides slowly diffuse into the surrounding cytosol. Control experiments were carried out to confirm that change in fluorescence is not due to the movement of the GNPs themselves during activation.

After validating steps essential in using ONCOS, we carried out ONCOS in breast carcinoma cells to block the mRNA translation of ERBB2, an oncoprotein commonly overexpressed in 20–30% of breast cancers.⁴⁰ General transfection methods of bringing DNA into cells, such as viral vectors or cationic liposome-mediated transfection, lack the spatial and temporal control of gene interference. Nevertheless, as a conventional measure of gene interference, a multicomponent lipid-based transfection reagent was used to initially determine the optimal modulation of ERBB2 expression in BT474 breast carcinoma cells by antisense oligonucleotides. ERBB2 receptors are stained with fluorescently labeled antibodies against ERBB2. Flow cytometry results show that there is no significant change in expression 24 h after transfection (Supporting Information Figure S3a). However, for 9.0% of transfected cells, the ERBB2 levels dropped below threshold after 48 h (Supporting Information Figure S2b).

After characterizing the experimental parameters for conventional gene interference of ERBB2, conjugated GNPs are internalized within cultured BT474 breast carcinoma cells. It has been suggested that there are between 168 and 336 ERBB2 molecules per cell.⁴¹ Since we estimate that each GNP releases approximately 250 molecules of oligonucleotides, we expect to see a difference in expression since there should be enough released oligonucleotides to bind with ERBB2 mRNA. To initiate photothermal gene release, an unfocused NIR laser is used to illuminate an entire population of cells. The cells are then allowed to culture for 48 h. Three control experiments are conducted to ensure that ONCOS activation is the reason for gene interference: cells which have internalized conjugated GNPs but have not been exposed to NIR illumination (Figure 5a), cells which do not contain GNPs but are exposed to NIR illumination (Figure 5b), and cells containing GNPs carriers of a scrambled sequence and have been exposed to NIR light (Figure 5c). If ONCOS is in fact inhibiting ERBB2 expression, control samples should express ERBB2 (Figure 5a–c) while ONCOS-activated cells should not (Figure 5d). To quantitatively analyze ERBB2 inhibition, ONCOS-activated cells and both control samples are stained with PE-labeled antibodies against ERBB2, and their fluorescence is analyzed by flow cytometry. The flow cytometric results (mean μ , coefficient

of variation CV, percent cells whose protein levels which have dropped below threshold) for the ONCOS-activated sample and both control samples are summarized in a table in Figure 5e. Figure 5 shows that for 13.2% of the cells treated with ONCOS, the protein levels dropped below threshold. It is especially noteworthy to point out that the average ERBB2 protein level of the entire cell population decreased by 55% after ONCOS activation. In Figure 5, the average fluorescence intensity of the control sample (contains no GNPs but illuminated with light) is 178.6 au and the average fluorescence intensity of the ONCOS-activated sample is 79.5 au. The average fluorescence intensity of the control sample which contains GNPs but is not illuminated with light is 199.4 au. To qualitatively visualize ERBB2 inhibition, the cells are fixed and immunostained with fluorescently labeled antibodies against the ERBB2 (Figure 5c,d). The decrease in fluorescence in the ONCOS-activated cells versus the control sample indicates that ONCOS has effectively interfered with ERBB2 gene expression.

Finally, in order for ONCOS to be used as a spatially and temporally controlled gene interference method, viability after ONCOS activation is crucial. Calcein AM, a dye which converts from nonfluorescent cell-permeant calcein AM into fluorescent calcein by intracellular esterase enzymes in living cells, is used as a measure of cell viability. Flow cytometry is used to analyze the samples 2 and 5 days after activation. As a control for the Calcein AM dye, cells are intentionally killed using sonication and stained with calcein AM. Two days after activation, cell samples show between 96–99% viability. Five days after activation, cell samples show between 93–97% viability (Figure 6a). There is only 2–3% variation in the viability between the control sample which contains GNPs but has not been exposed to light, the control sample which does not contain GNPs but has been exposed to light, and the ONCOS-activated sample. A representative DIC image and fluorescent image (live cells stained with Calcein AM, dead cells stained with Ethidium homodimer) of the ONCOS-activated sample is shown in Figure 6b,c and confirms the efficacy of ONCOS.

As the flow cytometric results for conventional transfection (Supporting Information Figure S2) and ONCOS-activated gene interference (Figure 5) indicate, the delivery of oligonucleotides into the cell with high efficiency remains challenging. It is however conceivable that this limitation can be overcome. For example, magnetic field driving of GNPs containing magnetic cores may be used to penetrate cell membranes with high efficiency.⁴² Once inside the cells, ONCOS can be activated with high efficiency. Future work in more efficient delivery of ONCOS carriers is currently underway. However, ONCOS still has several key advantages over conventional methods to inhibit protein translation. Whereas various methods can interfere with gene expression within a population of cells, precise control of a single cell's gene expression is not feasible. ONCOS can be activated to release oligonucleotides within a single cell, enabling the precise regulation of stochastic gene expression to better understand and control cellular signaling pathways. Furthermore, ONCOS provides a temporally controlled optical

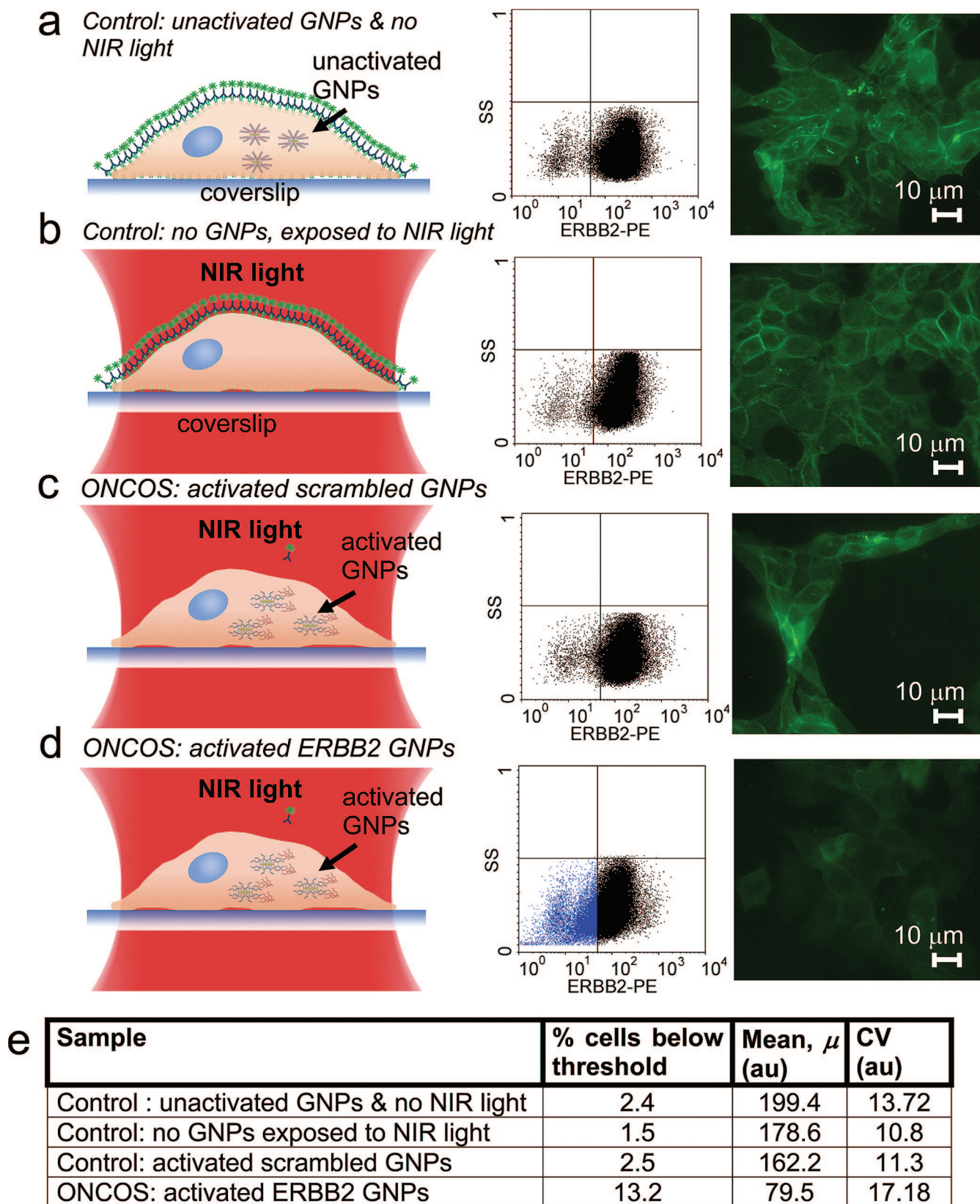


Figure 5. ERBB2 gene interference by ONCOS. (a) Concept, flow cytometric results, and representative image of indirect immunofluorescent staining of ERBB2 after 48 h in control cells which have been treated with conjugated GNP carriers but have not been exposed to NIR light. (b) Concept, flow cytometric results, and representative image of indirect immunofluorescent staining of ERBB2 after 48 h in control cells which do not contain conjugated GNP carriers but have been exposed to light. (c) Concept, flow cytometric results, and representative image of indirect immunofluorescent staining of ERBB2 in light-activated cells containing GNP carriers functionalized with scrambled sequences. (d) Concept, flow cytometric results, and representative image of indirect immunofluorescent staining of ERBB2 in ONCOS-activated ERBB2 knockdown in BT474 breast carcinoma cells. (e) Table summarizing flow cytometric results by percent of cells whose protein levels have dropped below threshold, average fluorescence intensity μ (au), and coefficient of variation CV (au).

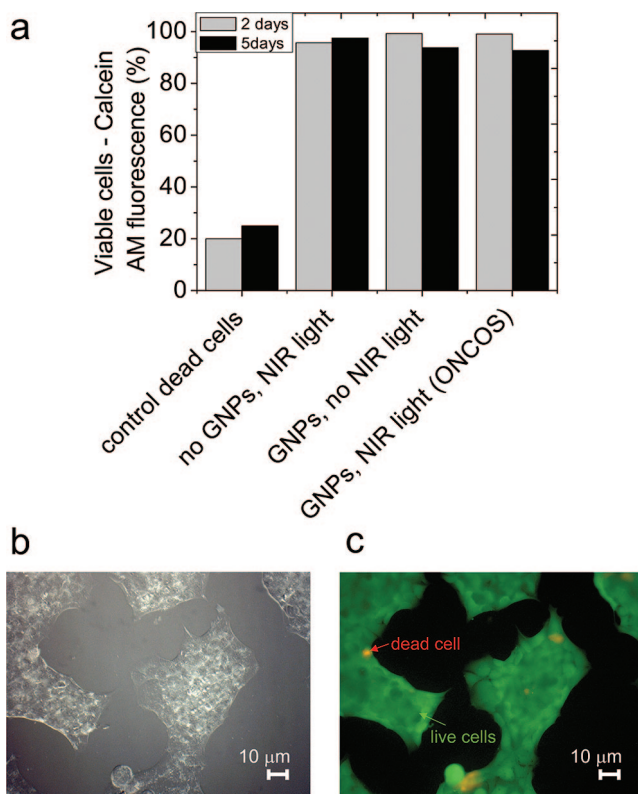


Figure 6. ERBB2 gene interference by ONCOS. (a) Calcein AM, a dye which converts from nonfluorescent cell-permeant calcein AM into fluorescent calcein by intracellular esterase enzymes in living cells, is used as a measure of cell viability. Flow cytometry is used to analyze the samples 2 and 5 days after activation. (b) Representative DIC image of BT474 cells after ONCOS activation. (c) Representative fluorescence image of live/dead cells after ONCOS activation. Live cells are stained with Calcein AM (green). Dead cells are stained with Ethidium homodimer (red).

switch to precisely regulate a single cell's gene expression and study its effect on an entire system. Finally, unlike other nanoparticle-based gene interference methods, ONCOS can achieve nanometer-scale spatial resolution while maintaining high cell viability due to the low temperature mechanism of release.

In summary, we have designed a nanoscale biophotonic transmitter and receiver system, ONCOS, which can interfere with gene expression in a single cell for applications requiring nanometer-scale targeted release and precise temporal control of release. Using ONCOS, it is possible to gain more control and flexibility in genetics, systems biology, and molecular cell biology-related studies. Gene interference can be programmed at a desired phase of a cell cycle or a certain moment after external growth factor stimulation, making it possible to study dynamic changes in translational events and gene expression that would normally be hidden by ensemble averaging of bulk population response.

Acknowledgment. The authors acknowledge National Institutes of Health (NIH) Nanomedicine Development Centers funding (3PN2 EY01824), National Academies Keck Futures Initiative funding (NAKFI Nano09), and the

Center for Nanostructure Materials Technology (CNMT) under the 21st century frontier R&D programs of the Korean Ministry of Science and Technology for financial support of the project. The authors acknowledge the National Physical Science Consortium (NPSC) graduate fellowship for support of S.E.L. The authors thank Yitao Long and Terry Johnson for technical insight. The authors also thank undergraduate students, Shalini Indrakanti and Daniel Yoo, for assistance with transfection and cell culture experiments.

Supporting Information Available: Detailed description of the materials and methods. This material is available free of charge via the Internet at <http://pubs.acs.org>.

References

- (1) Bahcall, O. *Mol. Syst. Biol.* **2005**, *1*, E1–E2.
- (2) Brent, R. *Nat. Biotechnol.* **2004**, *22*, 1211–1214.
- (3) Vance, V.; Vaucheret, H. *Science* **2001**, *292*, 2277–2280.
- (4) Rosenfeld, N.; Young, J. W.; Alon, U.; Swain, P. S.; Elowitz, M. B. *Science* **2005**, *307*, 1962–1965.
- (5) Gardner, T. S.; Cantor, C. R.; Collins, J. J. *Nature* **2000**, *403*, 339–342.
- (6) Nie, S.; Xing, Y.; Kim, G. J.; Simons, J. W. *Annu. Rev. Biomed. Eng.* **2007**, *9*, 12.112.32.
- (7) Hamad-Schifferli, K.; Schwartz, J. J.; Santos, A. T.; Zhang, S.; Jacobsen, J. M. *Nature* **2002**, *415*, 152–155.
- (8) Monroe, W.; McQuain, M.; Chang, M.; Alexander, J.; Haselton, F. *J. Biol. Chem.* **1999**, *274*, 20895–20900.
- (9) Ando, H.; Furuta, T.; Tsien, R.; Okamoto, H. *Nat. Genet.* **2001**, *28*, 317–325.
- (10) Shah, S.; Rangarajan, S.; Friedman, S. *Angew. Chem., Int. Ed.* **2005**, *44*, 1328–1332.
- (11) Asanuma, H.; Yoshida, T.; Ito, T.; Komiyama, M. *Tetrahedr. Lett.* **1999**, *40*, 7995–7998.
- (12) Liu, D.; Karanickolas, J.; Yu, C.; Zhang, Z.; Woolley, G. A. *Bioorg. Med. Chem. Lett.* **1997**, *7*, 2677–2680.
- (13) Rosi, N. L.; Giljohann, D. A.; Thaxton, C. S.; Lytton-Jean, A. K. R.; Han, M. S.; Mirkin, C. A. *Science* **2006**, *312*, 1027–1030.
- (14) Howard, K. A.; Dong, M.; Oupicky, D.; Bisht, H. S.; Buss, C.; Besenbacher, F.; Kjems, J. *Small* **2006**, *1*, 54–57.
- (15) Chen, C. C.; Lin, Y. P.; Wang, C. W.; Tzeng, H. C.; Wu, C. H.; Chen, Y. C.; Chen, C. P.; Chen, L. C.; Wu, Y. C. *J. Am. Chem. Soc.* **2006**, *128*, 3709–3715.
- (16) Horiguchi, Y.; Niidome, T.; Yamada, S.; Nakashima, N.; Niidome, Y. *Chem. Lett.* **2007**, *36*, 952–953.
- (17) Hirsch, L. R.; Stafford, R. J.; Bankson, J. A.; Sershen, S. R.; Price, R. E.; Hazle, J. D.; Halas, N. J.; West, J. L. *Proc. Second Joint EMBS/BMES Conf.* **2002**, *1*, 530.
- (18) Norman, R.; Stone, J.; Gole, A.; Murphy, C.; Sabo-Attwood, T. *Nano Lett.* **2008**, *8*, 302–306.
- (19) Pissuwan, D.; Valenzuela, S.; Killingsworth, M.; Xu, X. *J. Nanopart. Res.* **2007**, *9*, 1109–1124.
- (20) Loo, C.; Hirsch, L.; Lee, M.; Chang, E.; West, J.; Halas, N.; Drezek, R. *Opt. Lett.* **2005**, *30*, 1012–1014.
- (21) Tang, L.; Liu, L.; Elwing, H. *J. Colloid Interface Sci.* **1998**, *41*, 333–340.
- (22) Peterlinz, K. A.; Georgiadis, R. M. *J. Am. Chem. Soc.* **1997**, *119*, 3401–3402.
- (23) Liu, G. L.; Kim, J.; Lee, L. P. *Nat. Mater.* **2006**, *5*, 27–32.
- (24) Sershen, S. R.; Westcott, S. L.; Halas, N. J.; West, J. L. *Appl. Phys. Lett.* **2002**, *80*, 4609–4611.
- (25) Link, S.; El-Sayed, M. A. *Int. Rev. Phys. Chem.* **2000**, *19*, 409–453.
- (26) Huang, X.; El-Sayed, I. H.; Qian, W.; El-Sayed, M. A. *J. Am. Chem. Soc.* **2006**, *128*, 2115–2120.
- (27) Khlebtsov, B.; Zharov, V.; Melnikov, A.; Tuchin, V.; Khlebtsov, N. *Nanotechnology* **2006**, *17*, 5167–5179.
- (28) Cortie, M.; Xu, X.; Chowdhury, H.; Zareie, H.; Smith, G. *Proc. SPIE-Int. Soc. Opt. Eng.* **2005**, *5649*, 565–573.
- (29) Lu, Y.; Liu, G. L.; Kim, J.; Meija, Y. X.; Lee, L. P. *Nano Lett.* **2005**, *5*, 119–124.
- (30) Lee, E.; Liu, G. L.; Lee, L. P. *2006 Micro Total Analysis Systems (μ TAS)*, Tokyo, Japan, November 5–9, 2006.

- (31) Skirtach, A.; Dejugnat, C.; Braun, D.; Susha, A.; Rogach, A.; Parak, W.; Mohwald, H.; Sukhorukov, G. *Nano Lett.* **2005**, *5*, 1371–1377.
- (32) Skirtach, A.; Karageorgiev, P.; De Geest, B.; Pazos-Perez, N.; Braun, D.; Sukhorukov, G. *Adv. Mater.* **2008**, *20*, 506–510.
- (33) Nikoobakht, B.; El-Sayed, M. A. *Chem. Mater.* **2003**, *15*, 1957–1962.
- (34) Gou, L.; Murphy, C. J. *Chem. Mater.* **2005**, *17*, 3668–3672.
- (35) Sugimoto, C.; Segev, L.; Franke, T. *Metafectene method*. <http://www.biontexas.com>.
- (36) Iczkowski, K.; Omara-Opyene, A.; Klosel, R. *Mol. Biotechnol.* **2004**, *28*, 97–103.
- (37) Bonetta, L. *Nat. Methods* **2005**, *2*, 875–883.
- (38) Skirtach, A.; Javier, A.; Kreft, O.; Kohler, K.; Alberola, A.; Mohwald, H.; Parak, W.; Sukhorukov, G. *Angew. Chem., Int. Ed.* **2006**, *45*, 4612–4617.
- (39) Lukacs, G.; Haggie, P.; Seksek, O.; Lechardeur, D.; Freedman, N.; Verkman, A. *J. Biol. Chem.* **2000**, *275*, 1625–1629.
- (40) Guarneri, V.; Bengala, C.; Orlandini, C.; Gennari, A.; Donati, S.; Campani, D.; Collecchi, P.; Maur, M.; Conte, P. F. *Bone Marrow Transplant.* **2004**, *34*, 413–417.
- (41) Brandt, B.; Griwatz, C.; Heidl, S.; Assman, G.; Zanker, K. S. *Clin. Exp. Metastasis* **1996**, *14*, 399–408.
- (42) Cai, D.; Mataraza, J. M.; Qin, Z. H.; Huang, Z.; Huang, J.; Chiles, T. C.; Carnahan, D.; Kempa, K.; Ren, Z. *Nat. Methods* **2005**, *2*, 449–454.

NL802689K